19. RECORD-BREAKING HEAT IN NORTHWEST CHINA IN JULY 2015: ANALYSIS OF THE SEVERITY AND UNDERLYING CAUSES

CHIYUAN MIAO, QIAOHONG SUN, DONGXIAN KONG, AND QINGYUN DUAN

The record-breaking heat over northwest China in July 2015 was linked directly to atmospheric general circulation indices and anthropogenic forcing. The latter increased the risk of extreme heat by three-fold.

Introduction. In July 2015, northwest China experienced an unusually long and intense heat wave, especially in Xinjiang Autonomous Region (Fig. 19.1a). Maximum daily temperatures (TMX) exceeded 40°C on a record-breaking number of July days in 50 out of 88 counties in Xinjiang, and historical TMX records were broken in 28 counties. The highest TMX was 47.7°C in Turpan. This year also smashed the historical records of heat wave duration in 51 counties.

Our paper poses three questions: How extreme was the heat in Northwest China in July 2015 in a historical context? What factors led to the record-breaking heat? Did human-induced climate change increase the odds of abnormally high July heat in Xinjiang?

Data and methods. We collected the July TMX from National Meteorological Information Center (NMIC; http://data.cma.cn). The NMIC has conducted data quality control, including extreme value control, consistency check, and spatial consistency test (Liu and Li 2003). We used the data at the 53 stations with continuous July TMX records throughout the period of 1961–2015. We defined the extreme threshold as the 90th percentile of area-averaged July TMX between 1961 and 1990 (Mazdiyasni and AghaKouchak 2015). Heat wave duration was defined as the total number of days within July that TMX exceeded the threshold (Meehl and Tebaldi 2004).

Simulations from 10 global climate models (GCMs) from the Coupled Model Intercomparison Project Phase 5 of (CMIP5; Taylor et al. 2012) were used to assess the contribution of human influences on the observed July TMX (Supplemental Table S19.1 for the model list). The simulations driven by preindustrial control setting, natural forcing, all forcings, and anthropogenic greenhouse gases (GHG) forcing were assessed. As compared to the usual 2005, these 10 models extend the historical and natural simulations to 2012. However, we focused the GCM simulation analysis on the period 1961–2015 to enable comparison with observations. We used the TMX projection from the Representative Concentration Pathways 4.5 (RCP4.5) scenario to extend the time series of all forcings simulations through 2015, similar to Zhou et al. (2014) and Sun et al. (2014). For each GCM, only one member (r1i1p1) run was employed in this study. We used several statistical techniques to assess the severity and causes of the extreme heat:

1) To estimate the univariate return period, we selected the generalized extreme value (GEV) distribution for parametric fitting. This allows more stable estimates of return periods for extreme events occurring in the upper tail of the distribution (Fig. 19.1b). We used the Kolmogorov–Smirnov (K–S) goodness-of-fit test to verify the distribution (Wilks 2006).

2) We focused on the concurrence of July mean TMX anomaly and the duration of the heatwave (Fig. 19.1c). To estimate the concurrent extreme return period, we used the concept of copulas designed to model the dependence between multiple variables (Nelsen 2007). We used the Akaike information criterion (AIC; Akaike 1974) to identify the Gumbel copula as the most appropriate: smaller AIC values indicate a more reliable joint distribution (Supplemental Table S19.2).

3) To evaluate the impact of external forcing, we estimated scaling factors using the regularized optimal fingerprinting (ROF) method (Ribes et al.
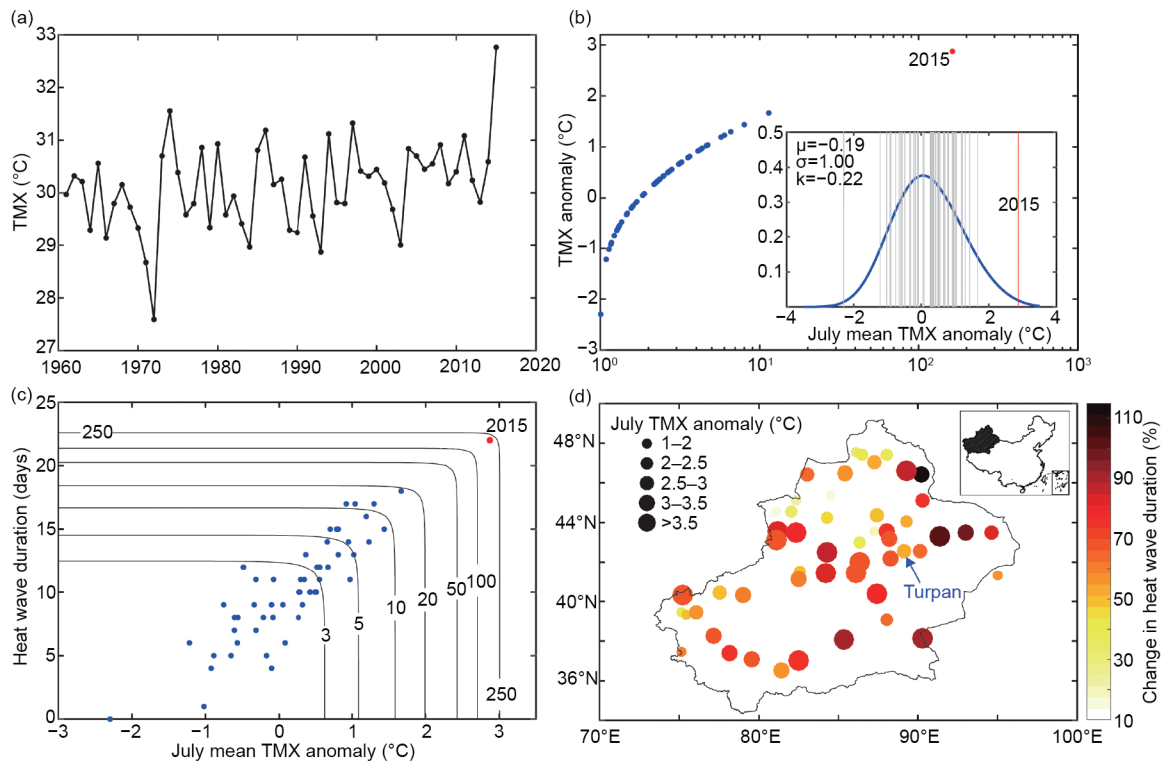
FIG. 19.1. (a) Time series of observed area-averaged Jul TMX over Xinjiang Autonomous Region, China, from 1961–2015. (b) Return period for Jul mean TMX. The univariate distribution was fit with a GEV function. Maximum likelihood estimates (MLEs) were used to obtain the location parameter μ, scale parameter σ, and shape parameter k. (c) Return period for concurrent Jul mean TMXs and heat wave durations. The bivariate joint distribution was fit with the Gumbel copula function. The numbers on the contour lines indicate the compound return period. (d) Spatial distribution of changes in July mean TMX anomaly (°C) and heat wave duration (%), relative to the average for each individual station during the baseline of 1961–90.

2013). Two categories were assessed: anthropogenic variations in GHG and natural forcing (Fig. 19.2b). Uncertainty ranges (5–95%) for the scaling factors were evaluated via Monte Carlo simulations. If the scaling factor for a forcing simulation was significantly greater than zero, then the influence of that forcing on the variable (i.e., July TMX) is detected (Zhang et al. 2013).

4) To analyze the attributable risk, we employed the conventional fraction of attributable risk (FAR = $1 - P_{nat}/P_{all}$) method (Stone and Allen 2005; Stott et al. 2015). We compared the probability of the observed 2015 July mean TMX anomaly occurring in the all forcing (P_{all}) and natural forcing (P_{nat}) simulations to ascertain the contribution of anthropogenic climate change. Bootstrapping (with replacement) was performed 1000 times per period to estimate the FAR uncertainty (Fig. 19.2c).

5) To test causality, we applied Granger causality analysis (GCA; Granger 1969). We examined the impact of the El Niño–Southern Oscillation (ENSO) on the monthly mean TMX during the period of 1961–2015 (Supplemental Fig. S19.1). The fundamental concept in GCA is that if the prediction of X (monthly mean TMX) is improved by including Y (here, the monthly ENSO index) as a predictor, then Y is said to be Granger causal for X (significance determined by F-test; $p < 0.05$; Sun et al. 2016). In addition, a contour map for the South Asia high (SAH) was generated to explore its coincidence with the heat events.

Results. A. Observed 2015 July TMX in historical context. Figure 19.1a shows that the July mean TMX in 2015 (32.76°C) was the highest during the past 55 years and was 2.87°C higher than the mean TMX during the baseline period (1961–90). The gray and red lines in the embedded figure in Fig. 19.1b correspond to July mean TMX anomaly during 1961–2014 and in 2015, respectively, relative to the baseline period. The K–S test shows that the GEV distribution was not rejected at $p < 0.05$ level. The 2015 July heat was close to a 1-in-166-year event. Because only 55 years of observed
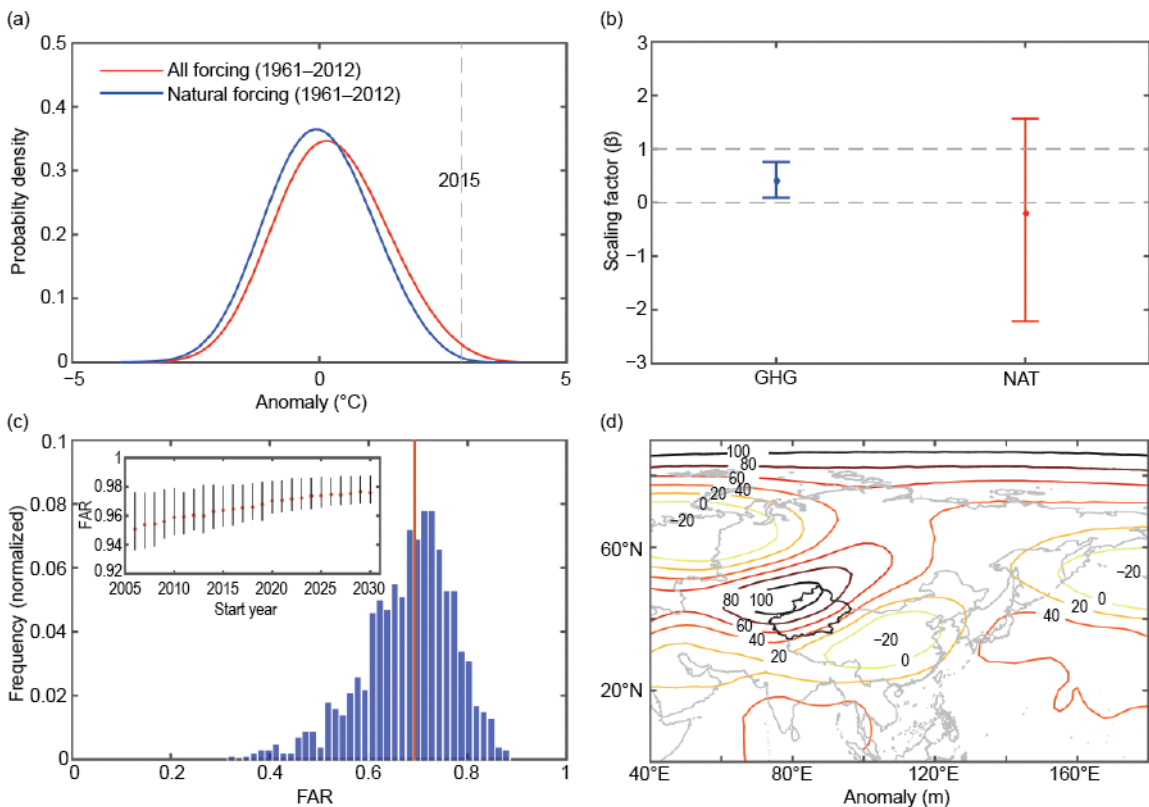
FIG. 19.2. (a) PDFs for Jul mean TMX anomaly (relative to 1961–90) for the all forcing (red) and natural forcing (blue) simulations; (b) Attribution analysis based on the TMX time series under different forcing conditions, (c) PDFs for estimated FAR focused on all forcing (1961–2015) and natural forcing (1961–2012). The blue histogram was generated by bootstrap resampling; the red line is the median. The embedded figure shows estimated FAR results (median and 25th–75th percentiles) from the all forcing simulation for different 30-year periods against the natural forcing simulation for 1961–2012. The x-axis indicates the starting year of the 30-year moving window. (d) The geopotential height anomaly field (m) for Jul 2015 at 100 hPa (baseline period: 1980–2009) estimated with the NCEP-DOE Reanalysis 2 datasets.

data were used, the 166-year return period can be considered as a lower bound. The blue and red dots in Fig. 19.1c indicate the return periods for concurrent July mean TMX and heat wave duration during the period 1961–2014 and in 2015. The July 2015 concurrency was a 1-in-200-year event. We also found that the most severe changes from baseline in 2015 July mean TMX and heatwave duration were mainly in the middle and northeastern areas of Xinjiang. The heat wave duration was approximately double that of the baseline period (Fig. 19.1d).

Results. B. Analysis of the attributable risk. We compared the likelihood of the July mean TMX anomaly occurring in different CMIP5 experiments (Fig. 19.2a). When anthropogenic forcing was included, the probability density function (PDF) shifted to the right, indicating an increased likelihood of high temperatures. The scaling factor for the GHG-forcing

simulation, estimated by the regularized optimal fingerprinting method, was 0.41 [90% confidence interval (CI): 0.09–0.76; Fig. 19.2b], suggesting that the changes in area-averaged July mean TMX were responsive to the anthropogenic greenhouse-gases forcing. It was estimated that all PDFs assumed a GEV distribution. When the 2015 July mean TMX anomaly (2.87°C) was marked as the threshold, the equivalent FAR value was 0.68 (90% CI: 0.51–0.81; Fig. 19.2c), indicating that 68% of the risk of such event is attributed to anthropogenic climate change. This translates to about three-fold (90% CI: 2.04–5.32) increase in the probability of 2015 July mean TMX anomaly occurring due to anthropogenic influence. The RCP4.5 experiments indicated that the risk from human-induced climate change increases with time, while uncertainty reduces with time (Fig. 19.2c, embedded figure). We also attempted to find other factors that contributed to the extremely high TMX

in July 2015. The 2015 ENSO was one of the strongest since 1960. GCA showed that there was no significant ($p = 0.35$) causal relationship between area-averaged mean TMX and ENSO index (Supplemental Fig. S19.1a). However, for 10 stations in central Xinjiang, significant causal relationship ($p < 0.05$) was detected between TMX changes and ENSO (Supplemental Fig. S19.1b). The extreme heat events in July 2015 might be also related to the movement of the South Asia high (SAH), which is the most intense and persistent anticyclone system in the upper troposphere and lower stratosphere over southern Asia during boreal summer (Mason and Anderson 1963). Less precipitation and heat events usually occur in the region where the SAH moves in (Chen et al. 2011). According to the geopotential height anomaly field in July 2015 at 100 hPa, the SAH center moved northward (Fig. 19.2d) and dominated the weather of the entire Xinjiang region, coinciding with the extreme heat events in northwest China.

Conclusions. Our analysis of July TMX records over the last 55 years indicates that the record-breaking heat observed over Northwest China in 2015 was at least a 1-in-166-year event. The return period increased to ~200 years if heat wave duration was also taken into account. CMIP5-based FAR analyses suggest that anthropogenic climate change increased the likelihood of such an extreme event by three-fold. The extreme heat event is related to the ENSO and SAH. This study is an important step toward a comprehensive understanding of the record-breaking 2015 heat in Xinjiang.

REFERENCES

Akaike, H., 1974: A new look to the statistical model identification. *IEEE Trans. Autom. Control*, **19**, 716–723.

Chen, L., S. G. Wang, K. Z. Shang, and D. B. Yang, 2011: Atmospheric circulation anomalies of large-scale extreme high temperature events in northwest china. *J. Desert Res.*, **31**, 1052–1058.

Granger, C. W. J., 1969: Investigating causal relations by econometric models and cross-spectral methods. *Econometrica*, **37**, 424–438.

Liu, X. M., and Q. X. Li, 2003: Research of the inhomogeneity test of climatological data series in China. *Acta Meteor. Sin.*, **17**, 492–502.

Mason R. B., and C. E. Anderson, 1963: The development and decay of the 100 mb summertime anticyclone over southern Asia. *Mon. Wea. Rev.*, **91**, 3–12.

Mazdiyasni, O., and A. AghaKouchak, 2015: Substantial increase in concurrent droughts and heatwaves in the United States. *Proc. Natl. Acad. Sci. USA*, **112**, 11484–11489, doi:10.1073/pnas.1422945112.

Meehl, G. A., and C. Tebaldi, 2004: More intense, more frequent, and longer lasting heat waves in the 21st century. *Science*, **305**, 994–997.

Nelsen, R. B., 2007: *An Introduction to Copulas*. Springer, 269 pp.

Ribes, A., S. Planton, and L. Terray, 2013: Application of regularised optimal fingerprinting to attribution. Part I: Method, properties and idealised analysis. *Climate Dyn.*, **41**, 2817–2836, doi:10.1007/s00382-013-1735-7.

Stone, D. A., and M. R. Allen, 2005: The end-to-end attribution problem: From emissions to impacts. *Climatic Change*, **71**, 303–318, doi:10.1007/s10584-005-6778-2.

Stott, P. A., 2015: Weather risks in a warming world. *Nat. Climate Change*, **5**, 517–518, doi:10.1038/nclimate2640.

Sun, Q., C. Miao, A. AghaKouchak, and Q. Duan, 2016: Century-scale causal relationships between global dry/wet conditions and the state of the Pacific and Atlantic Oceans. *Geophys. Res. Lett.*, **43**, 6528–6537, doi:10.1002/2016GL069628.

Sun, Y., X. Zhang, F. W. Zwiers, L. Song, H. Wan, T. Hu, H. Yin, and G. Ren, 2014: Rapid increase in the risk of extreme summer heat in Eastern China. *Nat. Climate Change*, **4**, 1082–1085, doi:10.1038/nclimate2410.

Taylor, K. E., R. J. Stouffer, and G. A. Meehl, 2012: An overview of CMIP5 and the experimental design. *Bull. Amer. Meteor. Soc.*, **95**, 485–498, doi:10.1175/BAMS-D-00094.1.

Wilks, D. S., 2006: *Statistical Methods in the Atmospheric Sciences*. International Geophysics Series, Vol. 91, Elsevier Academic Press, 627 pp.

Zhang, X. B., H. Wan, F. W. Zwiers, G. C. Hegerl, and S. K. Min, 2013: Attributing intensification of precipitation extremes to human influence. *Geophys. Res. Lett.*, **40**, 5252–5257, doi:10.1002/grl.51010.

Zhou, T. J., S. M. Ma, and L. W. Zou, 2014: Understanding a hot summer in central Eastern China: Summer 2013 in context of multimodel trend analysis [in "Explaining Extreme Events of 2013 from a Climate Perspective"]. *Bull. Amer. Meteor. Soc.*, **95 (9)**, S54–S57.